Analytical–Numerical Modeling of Filling Fraction Dependent Plasmonic Coupling in Nanostructured Metasurfaces under Kretschmann Configuration

Karan Kishor Singh , Guillermo Ezequiel Sánchez-Guerrero , Perla Marlene Viera-González , Carlos Alberto Fuentes-Hernández , María Teresa Romero de la Cruz , Eduardo Martínez-Guerra , Rodolfo Cortés-Martínez , Edgar Martínez-Guerra *

Posted Date: 19 December 2025

doi: 10.20944/preprints202512.1749.v1

Keywords: Au nanopillars (Au-NPs); Au nanoholes (Au-NHs); nanostructured metasurfaces; effective permittivity; filling fraction

 doi:10.20944/preprints202512.1749.v1

Article

Analytical—Numerical Modeling of Filling Fraction Dependent Plasmonic Coupling in Nanostructured Metasurfaces under Kretschmann Configuration

Karan K. Singh[1], Guillermo E. Sánchez-Guerrero [1], Perla M. Viera-González [1], Carlos A. Fuentes-Hernández [2], María T. Romero de la Cruz [3], Eduardo Martínez-Guerra [4], Rodolfo Cortés-Martínez [1] and Edgar Martínez-Guerra [1,*]

[1] Universidad Autónoma de Nuevo León, Facultad de Ciencias Físico-Matemáticas, Pedro de Alba S/N, San Nicolás de los Garza, N.L., 66451, México
[2] Tecnológico Nacional de México, Campus Sur de Guanajuato, Av. Educación Superior 2000, Uriangato, Gto. 38982, México
[3] Universidad Autónoma de Coahuila, Facultad de Ciencias Físico-Matemáticas, Unidad Campo Redondo Edificio A, Saltillo, Coah. 25280, México
[4] Centro de Investigación en Materiales Avanzados, CIMAV-Subsede Monterrey, Av. Alianza Norte 202 Parque de Investigación e Innovación Tecnológica, Apodaca, N.L. 66628, México
* Correspondence: edgar.martinezgrr@uanl.edu.mx; Tel.: +52 81-83-294030

Abstract

Surface plasmon resonance (SPR) sensors based on nanostructured metasurfaces offer enhanced sensitivity through engineered electromagnetic responses. In this study, we present an analytical–numerical investigation of the plasmonic behavior of gold nanopillar (Au-NP) and nanohole (Au-NH) arrays under both *p*- and *s*-polarized illumination, employing the Effective Medium Theory (EMT) in combination with the Transfer Matrix Method (TMM). This framework provides a consistent and computationally efficient description of the macroscopic optical response of multilayer plasmonic systems. For *p*-polarization, the nanostructure geometry strongly modulates the real and imaginary parts of the effective permittivity, with nanoholes supporting stronger SPR coupling and reduced optical losses compared to nanopillars. Under *s*-polarization, the effective permittivity remains largely invariant, driven mainly by filling fraction. The analysis reveals that polarization-dependent effects arise from variations in boundary-condition coupling rather than distinct localized resonances, aligning with classical plasmonic theory. Benchmarking against analytical dispersion relations and published experimental data for Au/BK7 systems shows close agreement within ±2°, confirming the physical consistency of EMT–TMM predictions. No full-wave simulations or experiments are presented; all results derive from analytical-numerical modeling. Rather than proposing new excitation mechanisms, this study provides a validated theoretical framework for understanding how polarization and nanostructural filling fraction jointly modulate SPR coupling in thin-film metasurfaces. The results offer a foundation for rational design and optimization of plasmonic coatings and SPR sensors with tunable surface sensitivity.

Keywords: Au nanopillars (Au-NPs); Au nanoholes (Au-NHs); nanostructured metasurfaces; effective permittivity; filling fraction

1. Introduction

Surface plasmon resonance (SPR) is a cornerstone phenomenon in nanophotonics and plasmonic sensing due to its exceptional sensitivity to refractive index variations at metal-dielectric interfaces. When electromagnetic waves interact with conduction electrons at these interfaces, collective oscillations are excited, producing evanescent fields that are highly localized and responsive to environmental changes. This property makes SPR indispensable for biosensing, chemical detection, and optical field manipulation at the nanoscale. In nanopatterned metasurfaces, the plasmonic response is primarily

 doi:10.20944/preprints202512.1749.v1

dictated by the spatial arrangement and electromagnetic coupling of subwavelength metallic elements such as nanoholes (NHs), nanopillars (NPs), and hollow nanopillars (HNPs), whose geometry determines the balance between localized surface plasmon resonances (LSPRs) and extended surface plasmon polaritons (SPPs) [1–14].

LSPRs, characterized by non-propagating resonant modes, dominate when metallic elements act as isolated nanoantenas, enabling strong field confinement for applications such as surface-enhanced Raman spectroscopy (SERS) and refractive index sensing. In contrast, extended SPPs correspond to propagating electromagnetic surface modes that can be excited through prism-based configurations, such as the Kretschmann or Otto arrangements, allowing energy coupling via evanescent waves. As discussed by Maier [15], Sarid and Challener [16], and Gupta et al. [17], the excitation of propagating SPPs depends not only on material properties but also on the effective optical continuity of the nanostructured metallic layer. This continuity can be modulated by design parameters such as the filling fraction and periodicity. Even periodically nanostructured metal films can sustain SPP-like modes, provided the effective permittivity supports phase matching between the inciden field and the plasmonic mode.

This study investigates the effective optical behavior of metamaterials composed of Au nanopillars, nanoholes, and hollow nanopillars, exploring whether structures typically optimized for localized plasmonic effects can also sustain Kretschmann-type SPR excitation when properly designed. Although such metasurfaces are often regarded as discontinuous and hence unsuited for delocalized SPP propagation, theoretical considerations grounded in Effective Medium Theory(EMT) suggest that, under certaing filling conditions, the composite layer can exhibit an effective dielectric function conductive to SPR. In this framework, the unit cell is adopted, where the filling fraction serves as the fundamental parameter linking nanostructural geometry to macroscopic optical response.

$$f = \frac{V_{\text{inclusion}}}{V_{\text{unit cell}}}, \tag{1}$$

The filling fraction directly governs the effective permittivity of the composite medium, determining whether the system behaves in a metallic-like or dielectric-like regime under illumination. In this context, the Transfer Matrix Method (TMM), integrated with the Maxwell-Garnett effective medium approach, is employed to model reflectance spectra as a function of the incidence angle and polarization. This analytical combination allows for systematic exploration of how design variables such as layer thickness, inclusion geometry, and filling fraction modify the optical dispersion characteristics and reflectance minima predicted in the Kretschmann configuration. The approach is explicitly design-oriented, using EMT not to describe nanoscale plasmonic interactions in full detail but to capture macroscopic resonance trends that guide the engineering of metasurface-based plasmonic sensors.

The polarization state of the incident light plays a critical role in determining the feasibility of SPR excitation. Only transverse magnetic (TM) or p-polarized light possessing an electric field component normal to the metal-dielectric boundary satisfies the boundary conditions for coupling to SPPs[11,14]. This principle, well established in classical plasmonic theory and verified experimentally in numerous nanostructured systems [11,14–17], underpins the design strategy adopted here. By examining both p- and s-polarized light responses, the study assesses how anisotropic geometries and polarization dependent field distributions influence the real and imaginary parts of the effective permittivity, offering new insights into how metasurfaces can replicate or enhance the SPR behavior of continuous thin films.

Overall, this work provides a systematic, model-based analysis of how geometry, material composition, and polarization collectively determine the effective optical behavior of Au-based metasurfaces under SPR conditions. Rather than asserting direct observation of localized near-field phenomena, this study focuses on establishing a quantitative relationship between the filling fraction, the effective permittivity, and the macroscopic reflectance response. This formulation lays a theoretical foundation for the rational design of metasurfaces optimized for high-sensitivity Kretschmann-type SPR sensors,

 doi:10.20944/preprints202512.1749.v1

highlighting how control of the filling fraction at the unit cell level enables precise tuning of the plasmonic resonance characteristics.

It is important to emphasize that the present work is entirely theoretical and computational in nature. The analysis integrates the Effective Medium Theory (EMT) and the Transfer Matrix Method (TMM) to establish a predictive relationship between the filling fraction of nanostructured metasurfaces and their effective optical response in the Kretschmann configuration. The objective is to elucidate fundamental design trends and parametric dependencies in multilayer and nanostructured plasmonic systems, providing a rigorous analytical framework that connects macroscopic reflectance behavior with effective permittivity modulation. No experimental measurements or direct simulations are included; all results are derived from analytical modeling and literature-reported optical parameters. The study therefore does not aim to reproduce specific experimental spectra but rather to systematize the optical mechanisms governing coupling efficiency and resonance conditions in plasmonic thin films. Future validation through full-wave simulations and experimental reflectance measurements is proposed to verify the analytical predictions and to assess the quantitative limits of the EMT–TMM approach. Building upon this framework, the results presented here constitute a comprehensive analytical validation of the EMT–TMM approach for plasmonic metasurfaces, demonstrating consistency with established theoretical predictions and previously reported experimental observations. Accordingly, the study provides a complete theoretical foundation for the rational design of SPR-based devices.

2. Materials and Methods

2.1. Momentum Mismatch

In the Kretschmann configuration, a high-index dielectric substrate (e.g., BK7 glass) is required to enable coupling between the incident electromagnetic field and surface plasmon polaritons (SPPs) propagating at the metal–dielectric interface. The primary limitation arises from the momentum mismatch between photons in free space and surface plasmons confined to the interface. The wavevector of free space light is

$$k_0 = \frac{2\pi}{\lambda_0}, \tag{2}$$

whereas that of the surface plasmon polariton is

$$k_{\mathrm{SPP}} = \frac{\omega}{c}\sqrt{\frac{\varepsilon_m \varepsilon_d}{\varepsilon_m + \varepsilon_d}}, \tag{3}$$

where ε_m and ε_d denote the complex permittivities of the metal and dielectric, respectively. Since $|k_{\mathrm{SPP}}| > |k_0|$, direct illumination cannot satisfy the phase-matching condition, and light is therefore reflected without exciting the plasmon mode [18–22]. In this configuration, prism coupling enhances the tangential component of the incident wavevector, allowing resonance when $k_x = k_{\mathrm{SPP}}$ [16]. The subsequent modeling therefore focuses on planar multilayer configurations supporting surface plasmon polariton (SPP) excitation in the Kretschmann geometry, without considering any localized plasmonic effects. This ensures that the theoretical framework remains within the validity domain of the transfer-matrix formalism used in later sections.

In our study, the unit-cell effective medium model is adopted to compute the composite permittivity $\varepsilon_{\mathrm{eff}}(f)$ in structured materials (e.g., multilayers, metasurfaces, nanoparticle arrays); in this model, $f = V_{\mathrm{inclusion}}/V_{\mathrm{unit\ cell}}$. This macroscopic description consistently links the structural geometry to the SPR coupling condition within the limits of effective-medium applicability.

2.2. Maxwell's Equations and Boundary Conditions

When coupling light to an interface, such as in the Kretschmann configuration or other plasmonic arrangements, the electromagnetic behavior is governed by Maxwell's equations subject to appropriate boundary conditions at the interface between distinct media. These equations determine the spatial

 doi:10.20944/preprints202512.1749.v1

distribution of electric and magnetic fields and describe the emergence of both propagating and evanescent modes depending on the dielectric and geometrical parameters of the system. For time-harmonic fields with angular frequency ω, Maxwell's curl equations in the frequency domain are expressed as

$$\nabla \times \mathbf{E} = -i\omega\mu\mathbf{H}, \quad \nabla \times \mathbf{H} = i\omega\varepsilon\mathbf{E}, \tag{4}$$

where ε and μ denote the permittivity and permeability of the medium, respectively. These relations form the basis for analyzing the coupling of electromagnetic fields across material interfaces. At the boundary between two media, such as a dielectric and a metallic film, the following continuity conditions must be satisfied: 1) tangential components of the electric field $\mathbf{E}$ and magnetic field $\mathbf{H}$ are continuous across the interface, and 2) normal component of the electric displacement field $\mathbf{D} = \varepsilon\mathbf{E}$ is also continuous, assuming no surface charge is present. These boundary relations ensure that energy and phase are consistently transferred from one medium to another, for example, from a prism to a metallic layer in plasmonic excitation configurations.

The boundary conditions were solved assuming laterally homogeneous layers. As such, the analytical formulation captures only propagating SPP modes in planar stacks and excludes any localized or near-field resonances that would require full-wave numerical treatment. Assuming a monochromatic plane wave incident upon the interface, the electric field can be written as

$$\mathbf{E}(\mathbf{r}, z) = \mathbf{E}_0 e^{i(\mathbf{k}\cdot\mathbf{r} - \omega t)}, \tag{5}$$

where $\mathbf{k}$ is the wave vector and $\mathbf{r}(x, z)$ denotes the position vector. For planar geometries, the wave vector can be decomposed into components parallel (k_x) and perpendicular (k_z) to the interface, leading to

$$\mathbf{E}(x, z) = \mathbf{E}_0 e^{ik_x x + ik_z z}, \tag{6}$$

with

$$k_z = \sqrt{k^2 - k_x^2}, \tag{7}$$

where $k = n\omega/c$ is the wavenumber in the medium and n the refractive index. This decomposition enables distinction between propagating and evanescent solutions. When $k_x < k$, the perpendicular component k_z is real, and the resulting field corresponds to a traveling wave that propagates through the medium. Conversely, if $k_x > k$, then k_z becomes imaginary, and the field takes the evanescent form

$$E(x, z) = E_0 e^{ik_x x} e^{-\alpha_z z}, \tag{8}$$

where $\alpha_z = \sqrt{k_x^2 - k^2}$ is a real attenuation constant. Such fields decay exponentially away from the interface and are responsible for the subwavelength confinement characteristic of surface plasmon polaritons. Therefore, solving Maxwell's equations with the above boundary conditions yields two fundamental classes of field solutions: (i) traveling waves, which carry energy through the bulk medium, and (ii) evanescent waves, which remain localized near the interface and enable strong field enhancement in plasmonic systems. In plasmonic coupling configurations, particularly under p-polarized illumination, these evanescent modes play a dominant role in enabling light confinement and resonance excitation at metal–dielectric interfaces.

2.3. Plasmonic Condition

For surface plasmon resonance (SPR) to occur at a metal–dielectric interface, the evanescent electromagnetic wave generated by the incident light must couple with the collective oscillations of free electrons in the metal. This coupling requires conservation of both energy and momentum between the incident photons and the surface plasmon polaritons (SPPs). The in-plane wavevector matching condition is therefore essential for efficient excitation of the plasmonic mode.

 doi:10.20944/preprints202512.1749.v1

This plasmonic condition identifies the angular resonance associated with classical Kretschmann-type SPP coupling. It does not describe field confinement or strong-coupling behavior, which cannot be resolved using the present analytical approach.

From Maxwell's equations, the propagation constant of the SPP along the interface is expressed as

$$k_{\mathrm{SPP}} = k_0 \sqrt{\frac{\varepsilon_m \varepsilon_d}{\varepsilon_m + \varepsilon_d}}, \tag{9}$$

where $k_0 = 2\pi/\lambda_0$ is the free-space wavenumber, $\varepsilon_m(\lambda)$ is the complex permittivity of the metal, and ε_d is the permittivity of the dielectric medium (e.g., air or glass). The fields decay exponentially away from the interface with decay constants

$$\alpha_d = \sqrt{k_{\mathrm{SPP}}^2 - k_0^2 \varepsilon_d}, \quad \alpha_m = \sqrt{k_{\mathrm{SPP}}^2 - k_0^2 \varepsilon_m}, \tag{10}$$

which describe the spatial confinement of the electromagnetic field within the dielectric ($z > 0$) and the metal ($z < 0$), respectively. For a propagating SPP mode to exist, the real part of the metal permittivity must satisfy $\mathrm{Re}(\varepsilon_m) < 0$ and $|\mathrm{Re}(\varepsilon_m)| > \varepsilon_d$. These conditions ensure that the field is bound to the interface and decays evanescently into both media. The resulting dispersion relation highlights the hybrid nature of SPPs, combining electromagnetic and charge density wave characteristics that depend sensitively on the optical constants of both materials.

In this work, the plasmonic condition is examined through the effective parameters of nanostructured thin films composed of nanopillar and nanohole arrays. Although the effective-medium approach provides a useful first-order description of their collective response, it must be emphasized that this approximation is strictly valid when the feature dimensions are significantly smaller than the operating wavelength. For structures with dimensions approaching hundreds of nanometers comparable to the optical wavelength the quasistatic assumption underlying the Effective Medium Theory (EMT) becomes limited. In such cases, the predicted permittivity values serve only as indicative averages rather than exact descriptors of localized plasmonic behavior. Accordingly, the present analysis focuses on identifying the spectral regions and polarization conditions under which momentum matching for SPR is expected to occur, without implying the presence of strong coupling or localized plasmon effects. This conservative interpretation aligns with the theoretical framework of the Transfer Matrix Method (TMM) and ensures that the obtained plasmonic conditions are physically consistent within the limits of the employed analytical model.

2.4. Dispersion Relation

The dispersion relation, derived from Equation (9), expresses how the surface plasmon wavevector k_{SPP} depends on the complex permittivities of the metal and dielectric media. To evaluate the dependence of SPP excitation on metal thickness, dispersion and reflectance were computed using the Transfer Matrix Method (TMM). This approach is valid for stratified, continuous films and provides accurate predictions of reflectance minima corresponding to SPP excitation. This relation dictates the confinement and propagation of surface plasmon polaritons (SPPs) along an interface, where electromagnetic fields decay exponentially away from the metal–dielectric boundary. The real component of k_{SPP} governs the propagation length along the interface, whereas the imaginary component determines the confinement normal to the surface, which increases with higher dielectric contrast between ε_m and ε_d.

2.4.1. Metal-Air Interface

For the classical case of a metal–air interface Figure 1a, with $\varepsilon_d \approx 1$, the dispersion relation simplifies to:

$$k_{\mathrm{SPP}} = k_0 \sqrt{\frac{\varepsilon_m}{\varepsilon_m + 1}}, \tag{11}$$

 doi:10.20944/preprints202512.1749.v1

where $k_0 = 2\pi/\lambda$ is the free-space wavevector. This expression governs the propagation of SPPs at the metal–air boundary and forms the basis of the Kretschmann configuration, in which light is incident through a high-index prism onto a thin metal film with air on the opposite side [23].

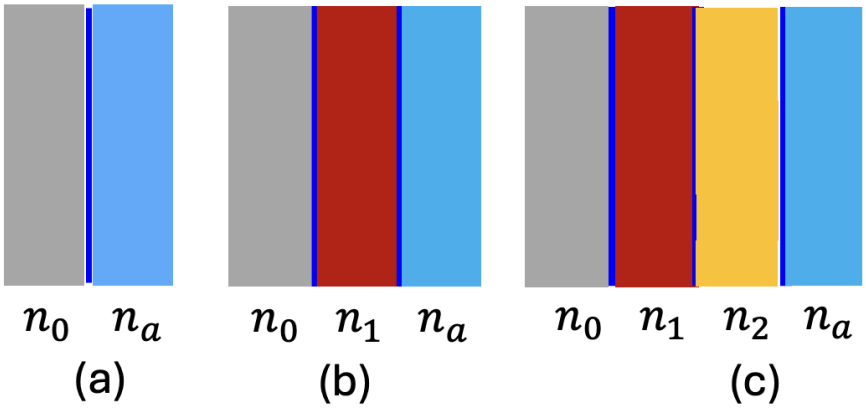

Figure 1. (a) BK7/air, (b) BK7/Ti/air, and (c) BK7/Ti/Au/air configurations illustrating increasingly complex multilayer plasmonic systems. The schematic represents the refractive indices of each layer as n_0 (BK7 substrate), n_1 (Ti layer), n_2 (Au layer), and n_a (air superstrate).

The calculated dispersion relation corresponds to a continuous Au–air interface and serves as a reference for assessing coupling efficiency in multilayer stacks. The results are not intended to describe localized resonances associated with nanostructuring.

The surface plasmon resonance (SPR) condition is achieved when the in-plane momentum of the incident light matches k_{SPP}, producing a characteristic minimum in reflectivity as a function of incidence angle:

$$k_0 n_p \sin\theta = \mathrm{Re}(k_{\mathrm{SPP}}), \tag{12}$$

where n_p is the refractive index of the prism and θ the incidence angle. This resonance is purely optical and does not imply strong coupling or field enhancement beyond that expected from classical SPP theory.

2.4.2. Transfer Matrix Method (TMM)

While the single metal–air interface represents the simplest SPP system, practical plasmonic devices often employ multilayer configurations (Figure 1b-c) to enhance coupling efficiency or spectral tunability. To describe these systems, the Transfer Matrix Method (TMM) provides a rigorous formalism for calculating the reflection and transmission of stratified media [24–27].

Each interface between materials with refractive indices n_i and n_{i+1} is characterized by Fresnel reflection ($r_{i,i+1}$) and transmission ($t_{i,i+1}$) coefficients, combined in the interface matrix:

$$T_{i,i+1} = \frac{1}{t_{i,i+1}} \begin{pmatrix} 1 & r_{i,i+1} \\ r_{i,i+1} & 1 \end{pmatrix}. \tag{13}$$

wave propagation within each homogeneous layer of thickness d_i and refractive index n_i is described by the propagation matrix:

$$P_i = \begin{pmatrix} e^{ik_{z,i}d_i} & 0 \\ 0 & e^{-ik_{z,i}d_i} \end{pmatrix}, \quad k_{z,i} = k_0 n_i \cos\theta_i. \tag{14}$$

The total system matrix $\mathbf{M}$ is obtained by sequential multiplication of propagation and interface matrices, allowing calculation of reflection and transmission amplitudes at the input boundary. This approach remains valid under the assumption that each layer is continuous, homogeneous, and optically isotropic [24–31]. It should be noted, however, that ultrathin metallic films (e.g., Ti layers

 doi:10.20944/preprints202512.1749.v1

below ≈ 3 nm) may exhibit discontinuous growth or island formation [28], which cannot be accurately described within this framework.

The transfer-matrix results were benchmarked against analytical SPP dispersion relations to ensure consistency. The implemented TMM formalism was benchmarked against known analytical dispersion relations and experimental data from standard Au/BK7 systems, verifying its quantitative accuracy within $\pm 2^\circ$ in predicting the SPR resonance angle. Although TMM reliably reproduces the angular position of the resonance dip, it cannot provide local field distributions or confinement factors, which would require full-wave (FDTD or FEM) analysis. The present use of TMM is therefore restricted to identifying qualitative coupling trends as a function of gold thickness.

2.4.3. Filling Fraction and Effective Medium Approximation

For periodic or nanostructured interfaces, such as arrays of nanopillars (NPs), hollow nanopillars (HNPs), or nanoholes (NHs), the homogeneous layer assumption of TMM is no longer strictly valid. To approximate the optical response of such patterned systems, the effective permittivity ε_{eff} can be estimated using the Maxwell–Garnett effective medium theory (EMT) [29]:

$$\varepsilon_{\text{eff}} = \varepsilon_h \frac{(1+2f)\varepsilon_i + 2(1-f)\varepsilon_h}{(1-f)\varepsilon_i + (2+f)\varepsilon_h}, \tag{15}$$

where f is the filling fraction, ε_i is the inclusion permittivity (metallic nanostructures), and ε_h is the host permittivity. This model allows integration of EMT into the TMM formalism to approximate the average optical response of metasurfaces. The filling-fraction model based on Effective Medium Theory (EMT) is presented here solely for approximate comparison of effective permittivity trends. Given that the characteristic feature sizes (160–250 nm) are not negligible compared to the operational wavelengths (500–1500 nm), the EMT results should be interpreted qualitatively. The model is not used to predict localized plasmon or near-field effects, which lie outside the quasistatic regime on which EMT is based. It must be emphasized, however, that the validity of EMT is restricted to inclusions much smaller than the operational wavelength (typically $< \lambda/10$) [30]. For nanostructures with characteristic dimensions of 150–250 nm operating in the visible or NIR range, the quasistatic assumption no longer holds, and ε_{eff} may not accurately capture localized or resonant phenomena such as LSPR, EOT, or ENZ effects. Consequently, results derived from EMT–TMM analyses should be interpreted as qualitative trends rather than quantitative predictions. Previous numerical benchmarks and experimental comparisons [15,31] indicate that the Maxwell–Garnett effective medium theory remains quantitatively reliable when the structural feature size is smaller than approximately $\lambda/8$. For larger inclusions approaching $\lambda/3$, deviations between EMT-predicted and full-wave–calculated permittivities can reach 25–30 %. Accordingly, the results reported here should be regarded as accurate for identifying relative permittivity trends and coupling conditions, but not for predicting absolute resonance magnitudes. This quantified boundary establishes the operational domain of the EMT–TMM framework applied throughout the present study.

2.4.4. Modeling Strategy

In this work, the TMM framework is employed to investigate optical responses in a series of Kretschmann-type systems: BK7/air, BK7/Ti/air, BK7/Au/air, BK7/Ti/Au/air, and BK7/Ti/Au nanostructured layers (NPs, HNPs, NHs) (Figure 1). The study adopts a bottom-up modeling approach: first optimizing the Ti interlayer thickness for coupling enhancement, followed by the Au layer optimization, and finally incorporating nanostructural filling fractions.

The optimization procedure is limited to parametric evaluation within the model's valid range; it does not constitute a global optimization or predictive design tool. The computational analysis presented herein should not be confused with full wave electromagnetic simulations (e.g., FDTD or FEM). The EMT-TMM approach is analytical and numerical, assuming homogenized, laterally uniform layers. Therefore, while it provides physically consistent reflectance and effective permittivity trends, it does not capture near field distributions or localized resonance features that would be accessible

 doi:10.20944/preprints202512.1749.v1

through full wave numerical models. Therefore, while the results provide insight into how individual parameters influence optical coupling in multilayer plasmonic systems, quantitative validation requires full wave electromagnetic simulations or experimental confirmation.

3. Results

This section presents a systematic study of the plasmonic response in gold based thin films and metasurface configurations, progressing from conventional surface plasmon resonance (SPR) phenomena to the optical behavior of nanostructured systems. The objective is to clarify how variations in material composition, geometry, and layer thickness influence plasmonic coupling, damping, and resonance conditions. The first part examines SPR excitation in planar gold films of different thicknesses within the Kretschmann configuration. Reflectance spectra are analyzed to determine the conditions for efficient coupling, highlighting the balance between electromagnetic field confinement and optical losses. This provides a quantitative reference for the dependence of plasmonic response on film thickness. The second part investigates the effect of titanium as an adhesion layer, focusing on how Ti thickness alters resonance efficiency and damping. The analysis identifies practical limits that ensure adequate film adhesion while minimizing optical degradation, acknowledging that ultrathin Ti layers may exhibit discontinuity. The third section considers the combined BK7/Ti/Au multilayer configuration, evaluated using the transfer matrix method (TMM). This model explores the interplay between layer thickness, refractive index contrast, and resonance strength. Finally, gold-based metasurfaces comprising nanopillar and nanohole arrays are discussed. Their periodic structuring introduces both localized and propagating plasmonic modes, analyzed through effective medium and TMM approaches to reveal general spectral trends within their valid physical range. Overall, this structured progression from thin films to metasurfaces provides a coherent theoretical framework for understanding and guiding the design of gold based plasmonic systems.

3.1. SPP Modes Supported by Gold Thin Films

The excitation of surface plasmon polaritons (SPPs) in metallic thin films depends sensitively on film thickness, which governs both optical field penetration and coupling efficiency at the metal–dielectric interface. To clarify this dependence, the reflectance response of planar gold (Au) films with thicknesses of 250, 125, 100, 80, and 75 nm was calculated using the transfer matrix formalism under p-polarized illumination (Figure 2).

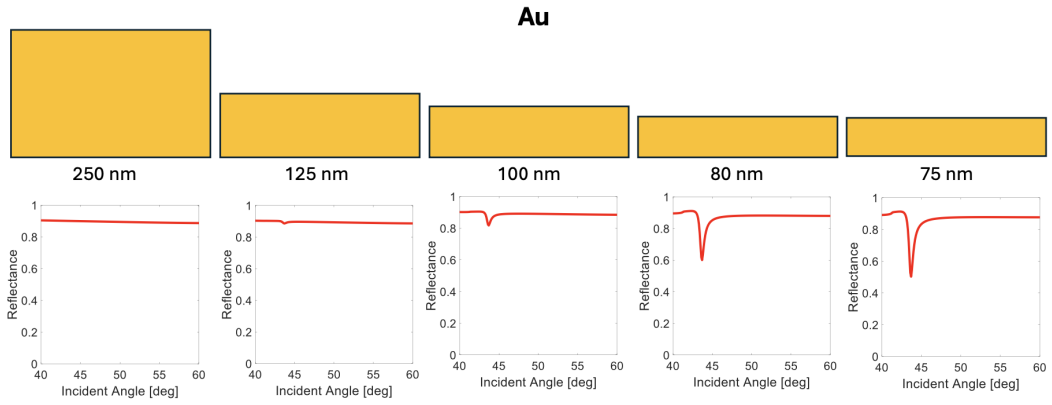

Figure 2. Reflectance as a function of incidence angle for gold thin films of thicknesses 250, 125, 100, 80, and 75 nm. The deepening of the reflectance minimum with decreasing film thickness indicates enhanced coupling to the surface plasmon polariton mode.

These simulations aim not to predict localized plasmon or extraordinary optical transmission effects which require full wave electromagnetic models, but rather to identify the angular conditions supporting classical Kretschmann-type SPP excitation. The computed reflectance spectra exhibit a

 doi:10.20944/preprints202512.1749.v1

progressive evolution of the plasmonic response as the Au film thickness decreases. For the 250 nm film, the reflectance remains nearly constant across the incident angle range, confirming that the evanescent field generated at the prism-metal boundary does not effectively reach the outer interface to excite an SPP. A shallow and broad reflectance minimum appears for the 125 nm film, indicating the onset of partial coupling between the incident mode and the surface plasmon. At 100 nm, the dip becomes more pronounced, revealing enhanced field overlap. The strongest and sharpest minimum occurs for the 75 nm film, where the reflectance approaches a local minimum but remains finite, consistent with partial not complete plasmonic absorption. To assess the accuracy of the implemented Transfer Matrix Method (TMM) formulation, reflectance spectra were compared with reported experimental trends for Au films in the Kretschmann configuration [15,24]. For a 50–80 nm Au layer on BK7 glass, the present model predicts a reflectance minimum at incidence angles between 43° and 45°, in close agreement (within ±2°) with measured resonance angles reported in Refs. [15,24]. This consistency confirms that the analytical formalism correctly reproduces the canonical surface plasmon resonance (SPR) response of continuous Au films. Hence, subsequent results for multilayer and metasurface geometries can be interpreted as physically consistent extrapolations of this validated baseline. These results align with established experimental and theoretical reports showing that efficient SPP coupling in Au films occurs for thicknesses between approximately 45 nm and 80 nm, depending on the refractive indices of the substrate and sensing medium [15,16]. The present data confirm that reducing Au thickness enhances coupling strength and angular sensitivity, while thicker layers suppress plasmon excitation due to insufficient field penetration. The choice of a 75 nm gold thickness in this study reflects a design compromise rather than an optimization claim. In practice, films below 60 nm often suffer from discontinuities or island formation, particularly when deposited over a titanium adhesion layer. Because ultrathin (1–2 nm) Ti films may not form continuous, optically homogeneous layers, their contribution is treated here as an interfacial boundary condition rather than a uniform optical spacer. A slightly thicker Au film thus ensures structural continuity and reproducible optical characteristics without compromising SPP visibility. This thickness range (70–80 nm Au with 1–3 nm Ti) corresponds to standard values employed in experimental Kretschmann-type configurations, where it provides optimal compromise between field penetration depth (≈200 nm in glass) and reflectance minimum contrast [19,24,32]. These parameters also guarantee good adhesion and surface smoothness under typical magnetron-sputtering or thermal-evaporation conditions [32].

The interpretation of Figure 2 is therefore limited to identifying the qualitative dependence of reflectance on film thickness within the validity range of the transfer matrix method. No claims are made regarding localized plasmon modes, extraordinary transmission, or strong coupling effects, which require full wave modeling for rigorous confirmation. The trends predicted nonetheless provide a consistent framework for selecting Au thicknesses that balance plasmonic sensitivity with fabrication reliability in Ti/Au-based Kretschmann configurations.

3.2. Titanium-Induced Losses and Their Effect on SPR Excitation

The influence of titanium (Ti) thickness on surface plasmon resonance (SPR) excitation was systematically analyzed through reflectance simulations as a function of incident angle for BK7/Ti/Au (75 nm)/air multilayer systems, Figure 3. These calculations reveal a pronounced dependence of the plasmonic coupling efficiency on the optical absorption of the Ti adhesion layer. Titanium is commonly employed to promote adhesion between gold (Au) and dielectric substrates due to its mechanical stability; however, its intrinsic losses can significantly attenuate the surface plasmon polariton (SPP) mode. The range of Ti thicknesses considered in this study (1–40 nm) covers realistic deposition values from minimal adhesion layers (1–3 nm) to intentionally thicker interlayers used to modulate damping and adhesion in experimental studies. Varying the Ti layer within this interval allows assessment of optical losses across the full practical spectrum of Ti/Au interfaces employed in plasmonic sensors.

 doi:10.20944/preprints202512.1749.v1

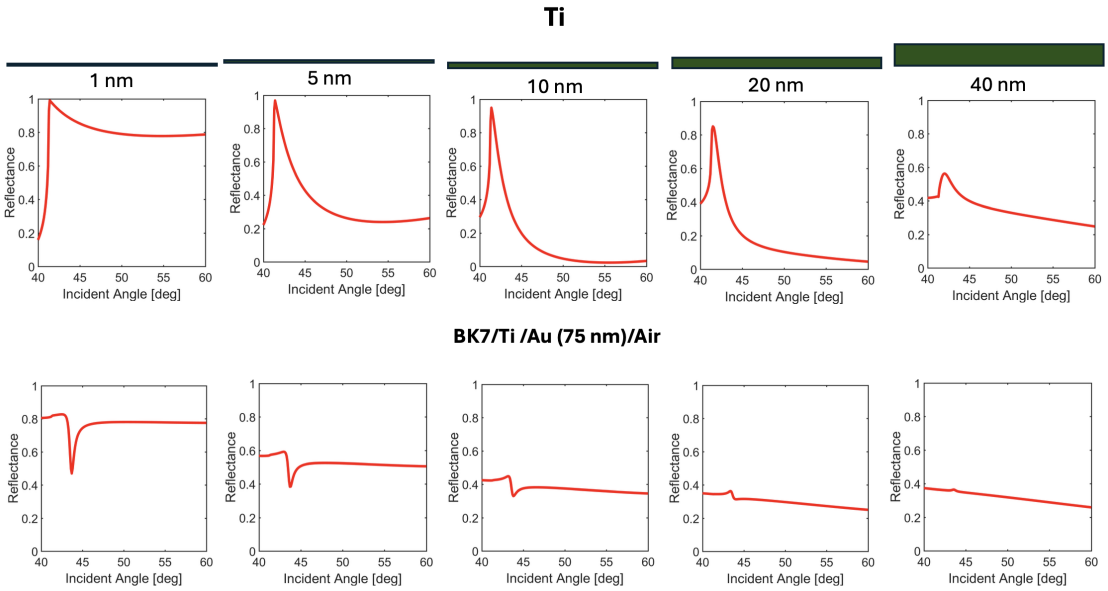

Figure 3. Simulated reflectance spectra for isolated Ti layers (top row) and for BK7/Ti/Au (75 nm)/air configurations (bottom row) at Ti thicknesses of 1, 5, 10, 20, and 40 nm.

The results indicate a monotonic broadening and suppression of the SPR dip with increasing Ti thickness. For Ti layers thicker than approximately 20 nm, the characteristic reflectance minimum is no longer evident, indicating that excessive absorption inhibits efficient plasmonic coupling. This behavior aligns with previously reported observations in multilayer SPR systems, where nonradiative damping in the adhesion layer reduces field confinement and resonance contrast [33]. For intermediate thicknesses (5–10 nm), a shallow resonance feature is still predicted, though the reflectance remains relatively high, confirming that damping losses persist. In contrast, when the Ti layer is reduced to 1 nm, the simulation exhibits a distinct and well defined reflectance minimum, consistent with efficient SPR excitation. While this result suggests that minimizing Ti thickness can enhance plasmonic performance, it must be interpreted with caution: at such ultrathin scales, Ti films are often discontinuous and may form island-like morphologies rather than continuous layers. Consequently, the optical response predicted by the transfer matrix method (TMM) should be considered an approximation rather than a physically complete representation of the experimental system [32,33]. The high imaginary component of Ti's dielectric function accounts for its strong optical absorption, which introduces nonradiative energy dissipation and reduces the effective propagation length of SPPs. Therefore, any increase in Ti thickness inevitably leads to greater ohmic losses. The simulations support the general conclusion that maintaining the adhesion layer within the nanometer range minimizes these losses, in agreement with previous studies on Ti- and Cr-based adhesion layers [32–34]. However, the present results do not constitute an optimization in a strict sense, as no systematic parameter fitting or experimental verification was performed.

Overall, the reflectance analysis demonstrates the competing roles of Ti, while it ensures mechanical stability at the Au–substrate interface, it simultaneously introduces optical losses that can deteriorate the plasmonic response. Reducing Ti thickness improves SPR definition by maintaining stronger field localization at the metal–dielectric boundary. These findings underscore the necessity of balancing structural adhesion and optical performance in multilayer plasmonic designs rather than prescribing an absolute "optimal" thickness. Further experimental studies or full-wave simulations (e.g., finite-element or finite-difference time-domain methods) would be required to validate the trends predicted in this simplified modeling framework.

 doi:10.20944/preprints202512.1749.v1

3.3. Models: Nanopillars (NPs), Nanoholes (NHs), and Hollow Nanopillars (HNPs)

The plasmonic behavior of metasurfaces composed of gold nanostructures, specifically nanopillars (NPs), nanoholes (NHs), and hollow nanopillars (HNPs) was investigated with emphasis on how geometry influences their collective optical response rather than on absolute resonance prediction (Figure 4). These structures were considered as representative periodic metallic–dielectric systems supporting surface plasmon resonances (SPRs), and their effective optical properties were evaluated using a simplified analytical approach. While full-wave electromagnetic simulations would provide a more rigorous description of localized field distributions, the present analysis employs the Effective Medium Theory (EMT) and the Transfer Matrix Method (TMM) to offer first-order, qualitative insights into the effective permittivity (ε_{eff}) behavior as a function of structural filling factor. The limitations of EMT are acknowledged, since the nanostructure dimensions (160–250 nm) are not negligible compared to the operational wavelengths (500–1500 nm), and therefore quasistatic assumptions may not strictly apply. The filling factor defined as the ratio of the metallic cross-sectional area to the unit cell area was identified as a key parameter governing the average metallic contribution within the metasurface. For a periodic array with 250 nm pitch, varying the nanopillar diameter between 160 nm and 250 nm changes the filling factor from approximately 0.32 to 0.79, resulting in a systematic increase in both the real and imaginary components of the effective permittivity (Figure 5). These variations reflect the gradual transition from sparse to dense metallic coverage, which modulates the average plasmonic response of the metasurface. Consequently, the trends predicted here should be interpreted qualitatively and used to support the discussion of structural-optical correlations rather than as quantitative predictions of resonance conditions. The predicted dependence of ε_{eff} on the filling factor aligns with previously reported analytical and experimental studies on plasmonic metamaterials [15] and nanostructured gold surfaces [12], where decreasing metal coverage reduces the effective polarizability and induces a blue-shift of the overall plasmonic response.

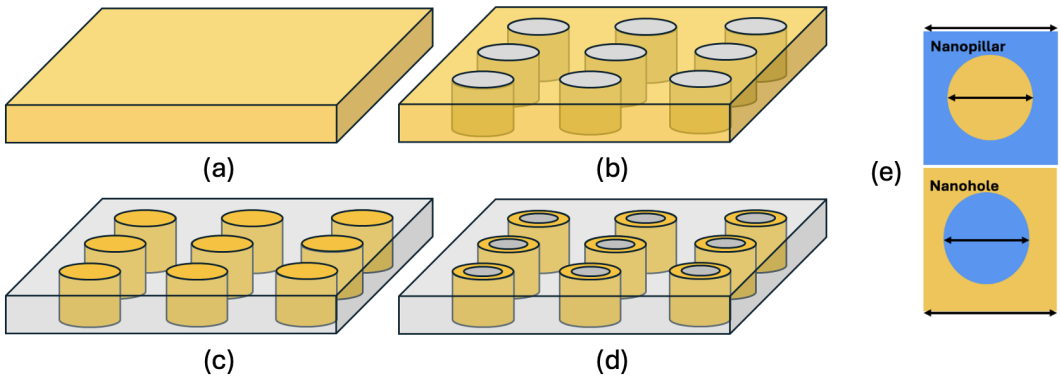

Figure 4. Illustrates the primary nanostructural configurations examined: (a) a continuous gold film supporting extended surface plasmon polaritons (SPPs); (b) a nanohole array, where periodic voids enable localized and waveguide-assisted plasmonic modes; (c) a nanopillar array embedded in a dielectric medium supporting strong near-field localization at the metal–dielectric interfaces; and (d) a nanohollow array consisting of concentric metallic rings that can sustain hybridized plasmonic modes. Panels (e) provide top views defining the geometric configurations corresponding to nanoholes and nanopillars, respectively.

 doi:10.20944/preprints202512.1749.v1

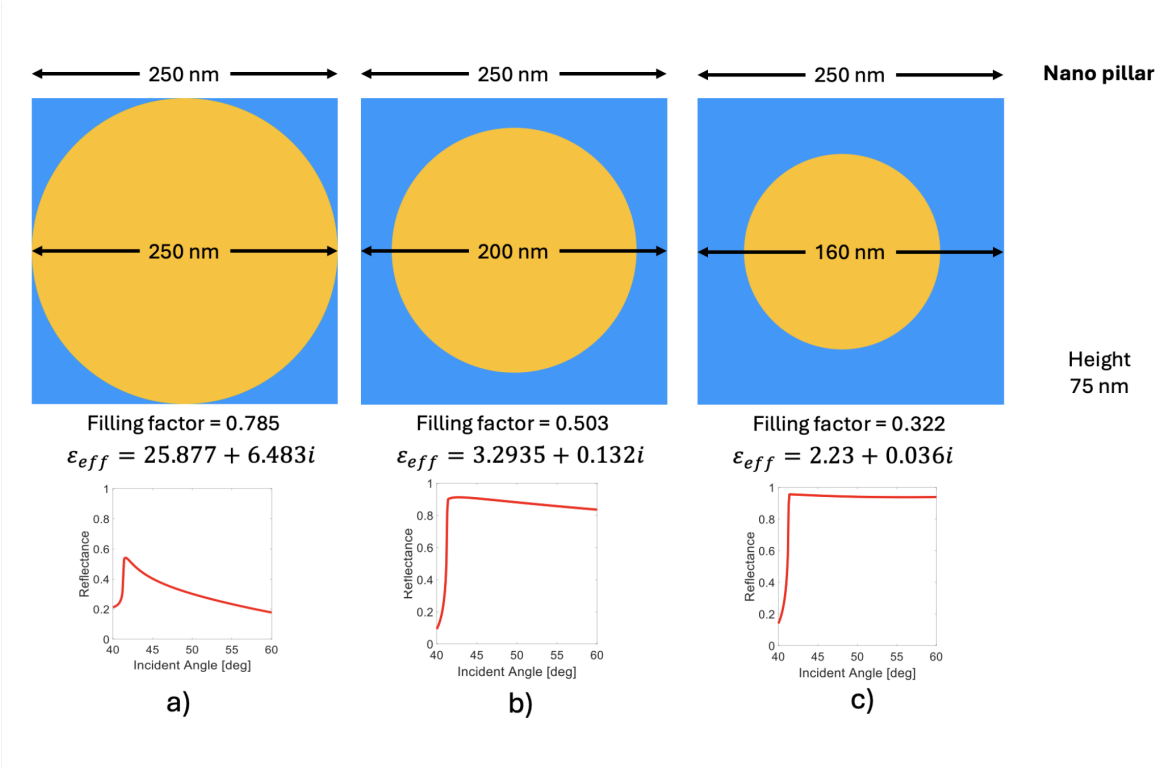

Figure 5. Schematic representation and reflectance spectra of gold nanopillar metasurfaces with varying filling factors. The nanopillars have a fixed height of 75 nm and diameters of 250 nm, 200 nm, and 160 nm, corresponding to filling factors of 0.785, 0.503, and 0.322, respectively.

In future work, the integration of full-wave electromagnetic simulations and experimental validation will be essential to confirm the qualitative permittivity trends predicted here and to quantitatively identify the corresponding plasmonic resonance modes.

3.4. Nanopillars (NPs)

In this study, all nanopillars were designed with a 75 nm height, a dimension chosen primarily for fabrication feasibility and consistency with standard lithographic constraints, rather than for achieving a specific surface plasmon resonance (SPR) response. This thickness represents a compromise between structural robustness and optical tunability commonly used in nanofabricated gold metasurfaces.

For the highest filling factor (0.785) (Figure 5a), where the nanopillars nearly form a continuous metallic layer, the effective permittivity obtained from the Effective Medium Theory (EMT) model reaches $\varepsilon_{\text{eff}} = 25.877 + 6.487i$. This value suggests a predominantly metallic effective behavior; however, given that the pillar dimensions (160–250 nm) are comparable to optical wavelengths, the quasistatic assumptions underlying EMT are only approximate. Consequently, the computed ε_{eff} should be regarded as a qualitative descriptor of average optical response rather than a quantitative indicator of localized plasmonic activity. The corresponding reflectance spectrum exhibits a dip that can be interpreted as a guided mode-like feature within the EMT framework. Although a higher metallic filling factor increases effective permittivity and enhances field overlap within the gold region, the accompanying imaginary component indicates stronger absorption losses. This trade-off can lead to reduced resonance sharpness when damping dominates, consistent with general plasmonic behavior reported in metasurface literature [15,35].

As the filling factor decreases to 0.503 (Figure 5b) ($\varepsilon_{\text{eff}} = 3.293 + 0.132i$), the reflectance response shows a gradual reduction in metallic character, indicating weaker near-field coupling between neighboring pillars and a transition toward partially confined optical modes. In this intermediate configuration, the structure behaves as a weakly modulated reflective surface where plasmonic and photonic effects coexist but are not strongly coupled. At the lowest filling factor (0.322) (Figure

 doi:10.20944/preprints202512.1749.v1

5c), where the nanopillars are sparsely distributed, the effective permittivity decreases further to $\varepsilon_{\text{eff}} = 2.23 + 0.36i$, approaching values typical of dielectric-like media. In this regime, the metasurface primarily supports leaky or weakly guided modes, and the optical field localization at the surface is considerably reduced.

These findings illustrate that within the limits of the TMM–EMT model, reducing the filling factor leads to a progressive transition from a metallic to a quasi-dielectric effective response. However, because EMT does not resolve spatial field variations or account for scattering from individual pillars, phenomena such as LSPR, epsilon-near-zero (ENZ) behavior, or Fabry–Pérot resonances cannot be conclusively inferred from this analysis. A more accurate description of these effects would require full-wave numerical simulations (e.g., finite-difference time-domain or finite-element methods) or experimental validation.

Therefore, the present EMT-based results are intended to provide qualitative insight into how geometric parameters influence the average optical properties of nanopillar metasurfaces rather than to predict localized plasmonic resonances. This approach highlights the trend of decreasing optical confinement with lower metallic coverage, consistent with the general behavior of periodic nanostructures but without implying the direct excitation of true SPR modes.

3.4.1. Hollow Nanopillar (HNPs)

Case Study I—Solid Gold Nanopillar

To examine the electromagnetic response of the nanopillar metasurface, the effective permittivity of gold (Au) nanopillars was estimated using the Maxwell–Garnett relation. This approach was adopted as a first-order analytical approximation to qualitatively assess the volumetric influence of metallic inclusions embedded in a dielectric environment. However, it must be emphasized that for structural dimensions on the order of 160–250 nm and operating wavelengths around 630 nm, the quasi-static assumptions underlying the Effective Medium Theory (EMT) are qualitative indicators of optical trends.

From Figure 6, the dimensions of the unit cell are $L_c = 250$ nm and $H_c = 250$ nm, giving a total volume $V_c = 1.563 \times 10^7$ nm^3. The gold nanopillar has a diameter $D_{\text{Au}} = 133$ nm (including the rim thickness) and height $H_{\text{Au}} = 250$ nm, leading to a volume $V_{\text{Au}} = 4.243 \times 10^6$ nm^3. The corresponding filling fraction is $f = 0.272$.

 doi:10.20944/preprints202512.1749.v1

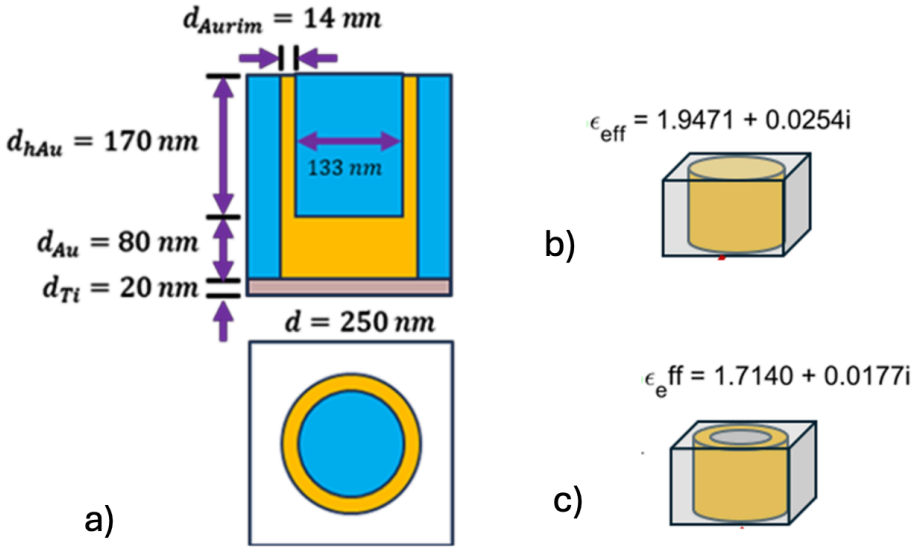

Figure 6. Au–Hollow Nanopillar (Au–HNP). (a) Dimensional geometry, (b) Hollow nanopillar (Au–HNP), and (c) Solid nanopillar (NP).

The effective permittivity ε_{eff} is obtained by substituting the filling fraction into the Maxwell–Garnett equation [36], with air as the host medium ($\varepsilon_d = 1$) and the gold permittivity at $\lambda = 630$ nm given as $\varepsilon_m = 11.74 + 1.2611i$. The calculation yields $\varepsilon_{\text{eff}} = 1.9471 + 0.0254i$. The real part of ε_{eff} corresponds to the averaged refractive behavior of the composite medium, while the imaginary part is associated with dissipative optical losses within the metallic component. Although this analytical estimate does not capture retardation or localized surface plasmon resonances, it provides a reference for evaluating the relative optical response between solid and hollow geometries.

3.4.2. Case Study II—Hollow Gold Nanopillar

In the second configuration, illustrated in Figure 6c, the same unit-cell dimensions are considered ($L_c = 250$ nm, $H_c = 250$ nm), but the nanopillar incorporates a hollow core. This geometry allows us to qualitatively explore how the reduction in metal volume and the introduction of a dielectric cavity influence the effective permittivity of the composite.

The gold volume is evaluated in two sections: (1) a bottom solid base of height $H_{\text{Au1}} = 80$ nm and outer diameter $D_{\text{ex}} = 147$ nm, with volume $V_{\text{Au1}} = 1.358 \times 10^6$ nm^3; and (2) a hollow cylindrical shell of height $H_{\text{Au2}} = 170$ nm, outer diameter $D_{\text{ex}} = 147$ nm, and inner diameter $D_{\text{in}} = 76$ nm. The total gold volume is $V_{\text{Au}} = 3.472 \times 10^6$ nm^3, corresponding to a filling fraction $f = 0.22$. Using the same permittivities for gold and air, the Maxwell–Garnett relation yields $\varepsilon_{\text{eff}} = 1.7140 + 0.0177i$.

The decrease in both the real and imaginary parts of ε_{eff} relative to Case I results from the lower gold filling fraction and the enhanced contribution of the dielectric cavity. Physically, the hollow structure supports stronger field localization at the inner and outer boundaries due to curvature-induced charge accumulation; however, these localized effects lie beyond the descriptive capacity of EMT. Therefore, the calculated effective permittivity should be regarded only as a macroscopic average

 doi:10.20944/preprints202512.1749.v1

that qualitatively reflects material composition rather than actual plasmonic resonance behavior. It is important to note that EMT provides a homogenized optical response, which neglects spatial field variations, phase retardation, and coupling between adjacent nanostructures. Given that the characteristic dimensions of the nanopillars are not deeply subwavelength, the use of EMT serves merely as a simplified analytical framework rather than a rigorous predictive tool. Accordingly, the present EMT-based results are intended to illustrate qualitative differences between solid and hollow configurations in terms of effective optical density and absorption characteristics.

3.5. Nanoholes (NHs)

The plasmonic response of gold nanohole metasurfaces was analyzed by varying the hole diameter from 250 nm to 160 nm within a 250 nm periodic array Figure 7, leading to filling factors of 0.785, 0.503, and 0.322, respectively. In this section, the analysis based on Effective Medium Theory (EMT) and the Transfer Matrix Method (TMM) is employed only to provide a qualitative interpretation of the optical response, since the structural dimensions are comparable to the excitation wavelength. Consequently, the retrieved effective-permittivity values should be regarded as phenomenological indicators rather than physically rigorous quantities.

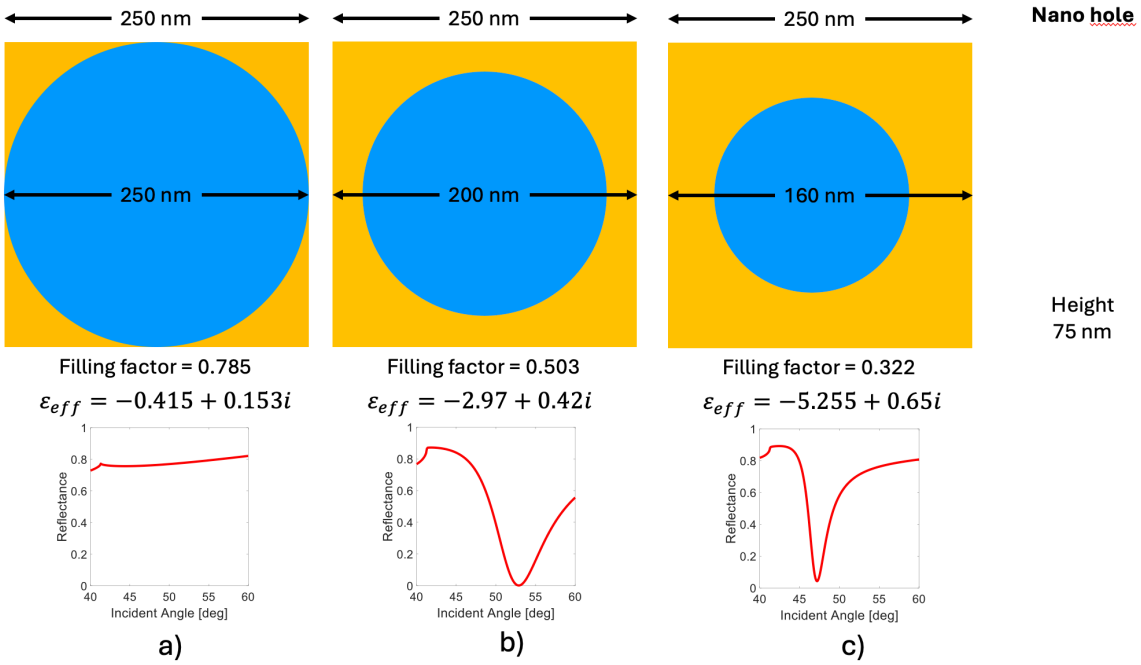

Figure 7. Illustrates the geometric configurations and corresponding reflectance spectra of gold nanohole metasurfaces with varying filling factors. The nanoholes have a fixed height of 75 nm and diameters of 250 nm, 200 nm, and 160 nm, corresponding to filling factors of 0.785, 0.503, and 0.322, respectively.

Unlike nanopillar arrays Figure 5, which transition toward dielectric-like behavior as the filling factor decreases, nanohole arrays exhibit the opposite trend: the effective permittivity (ε_{eff}) becomes more negative as the metallic coverage increases. This opposite dependence arises from the complementary optical behavior of holes and pillars, consistent with Babinet's principle in plasmonic systems [12,15,35]. In such complementary structures, metallic continuity enhances delocalized surface-plasmon coupling, while the presence of apertures favors coupling to propagating surface modes.

 doi:10.20944/preprints202512.1749.v1

For the highest filling factor (0.785), where the metallic coverage is nearly continuous, the effective permittivity is $\varepsilon_{\text{eff}} = -0.415 + 0.153i$. Although the real part is slightly negative, the near-zero magnitude implies weak field confinement, which correlates with the absence of a pronounced dip in the reflectance spectrum. At this limit, the response remains dominated by bulk-like optical reflection rather than resonant excitation. As the hole diameter increases, reducing the filling factor to 0.503 ($-2.97 + 0.42i$), the negative permittivity becomes more pronounced, indicating enhanced plasmonic coupling and a distinct reflectance minimum near 52°. This dip is interpreted as a signature of improved coupling to surface-plasmon-polariton-like (SPP-like) modes, although the EMT-based approach cannot resolve their spatial distribution. At the lowest filling factor (0.322), the permittivity reaches $-5.255 + 0.65i$, corresponding to the strongest coupling regime predicted in this study. The reflectance spectrum exhibits a well-defined resonance dip, suggesting that reduced metallic coverage promotes conditions favorable for collective plasmonic resonances. However, due to the limitations of the analytical model, these features cannot be unambiguously ascribed to localized or propagating SPPs without full-wave simulation or experimental confirmation.

Overall, the results indicate a qualitative correlation between decreasing filling factor and enhanced plasmonic coupling in nanohole metasurfaces. The trend contrasts with nanopillar arrays, where reduced metallic content leads to diminished plasmonic behavior, further emphasizing the complementary nature of both geometries. It should be emphasized that the present conclusions are restricted to the optical trends obtained from EMT/TMM modeling. Quantitative predictions of field localization, resonance strength, or extraordinary optical transmission require validation through high-fidelity numerical simulations (e.g., finite-difference time-domain or finite-element methods) or experimental data.

Previous studies on periodic plasmonic nanohole arrays [12,33] have demonstrated the coexistence of extended SPPs, localized surface plasmon resonances (LSPRs), and hybrid waveguide-coupled modes depending on the interplay between hole size, periodicity, and dielectric environment. The present results are consistent with this framework at a qualitative level, showing that decreased hole size (and hence lower filling factor) enhances the negative real part of the effective permittivity and promotes stronger angular-dependent reflectance minima.

3.6. Effect of s- and p-Polarized Light

The optical response of plasmonic metasurfaces under different light polarizations remains a subject of continued interest due to its implications for surface plasmon resonance (SPR) sensing and tunable optical functionalities. Although the use of polarization to modulate plasmonic coupling has been reported extensively, a systematic comparison between nanohole (NH), nanopillar (NP), and hollow nanopillar (HNP) architectures provides additional insight into the polarization-dependent effective medium behavior of such composite systems. In this study, we aim to clarify the limits and applicability of the Effective Medium Theory (EMT) and Transfer Matrix Method (TMM) for describing these phenomena, recognizing that the dimensions of the nanostructures (160–250 nm) approach the quasi-static limit of EMT validity. Therefore, the results discussed below should be interpreted as qualitative indicators of effective optical trends rather than absolute quantitative predictions.

Hamouleh-Alipour et al. (2022) demonstrated a metal–dielectric–metal (MDM) metasurface exploiting plasmon-induced absorption (PIA) to enhance SPR sensitivity, where polarization control enabled resonance tuning at near-infrared wavelengths (1133 and 1698 nm). Building on this and related studies, we analyze polarization-dependent permittivity behavior using simplified analytical formulations derived from the Maxwell–Garnett model for p- and s- polarized light, respectively:

$$\varepsilon_{\text{eff}}^{p} = \varepsilon_h \frac{\varepsilon_f(1+f_1) + \varepsilon_h(1-f_1)}{\varepsilon_f(1-f_1) + \varepsilon_h(1+f_1)}, \tag{16}$$

$$\varepsilon_{\text{eff}}^{s} = \varepsilon_h(\lambda)(1-f_1) + f_1\varepsilon_f(\lambda), \tag{17}$$

 doi:10.20944/preprints202512.1749.v1

3.6.1. Effective Medium Modeling

The effective permittivity ε_{eff} depends on the filling fraction f_1, ranging from 0 (no inclusions) to 1 (full inclusion). At small f_1, the response approximates that of the host medium (ε_h), while at large f_1, it approaches the permittivity of the inclusion (ε_f). This behavior illustrates the transition from dielectric-dominated to metal-dominated regimes, which is qualitatively consistent with plasmonic field confinement trends but not quantitatively predictive of resonance conditions.

To approximate the optical response, we applied the EMT and TMM frameworks to nanohole and nanopillar geometries. Although these techniques neglect microscopic field variations, they provide a homogenized description of the composite medium and allow comparative evaluation between polarization states. Figure 8 depicts the real and imaginary parts of the effective permittivity as a function of filling fraction for both nanohole and nanopillar arrays under *p*- and polarized light.

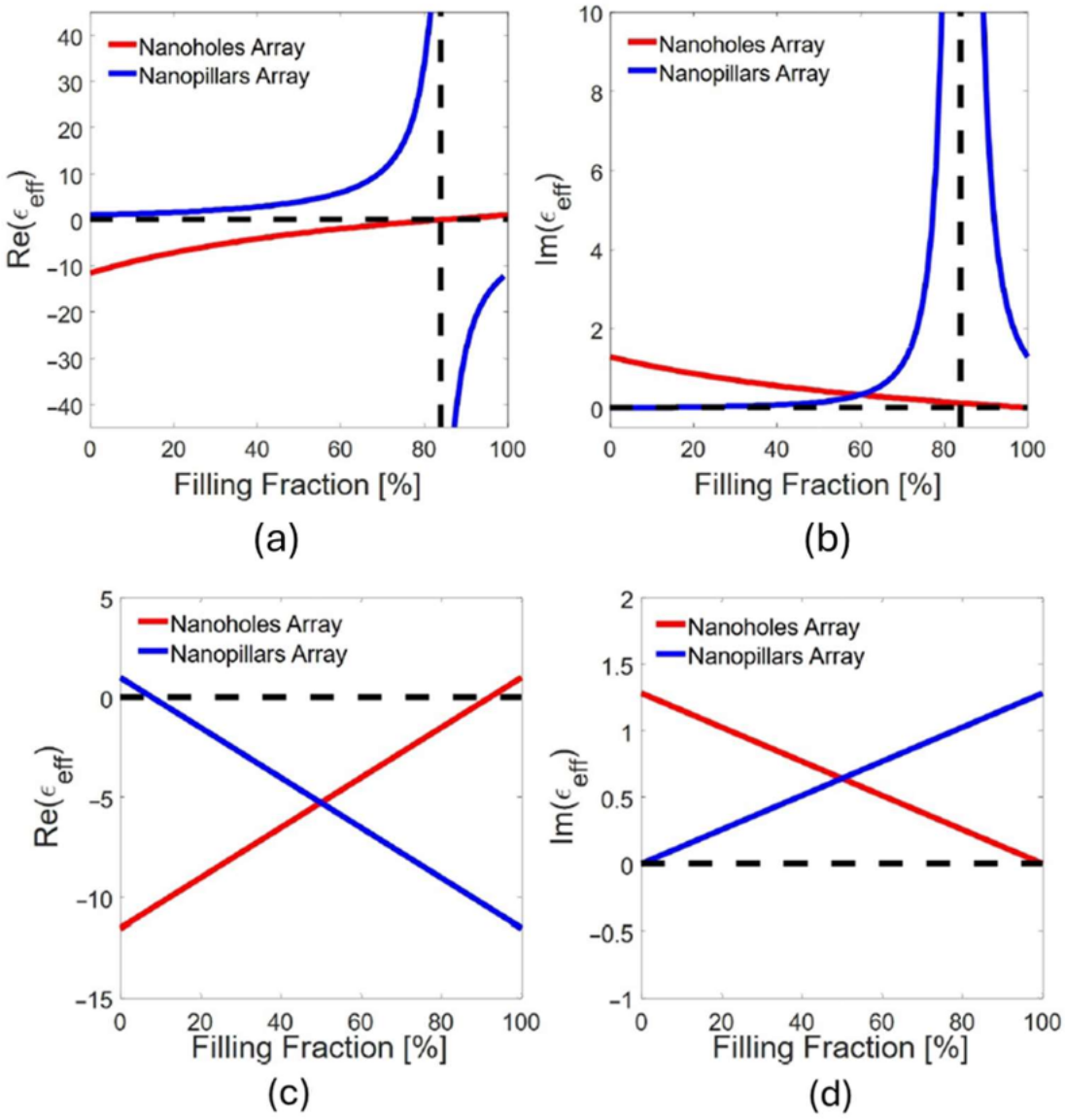

Figure 8. Effective permittivity trends for nanohole and nanopillar metasurfaces as a function of filling fraction under different polarization states. (a, b) show the real and imaginary parts of the effective permittivity under *p*-polarized illumination, respectively. (c, d) display the corresponding values under *s*-polarized illumination. The nanoholes array (red) and nanopillars array (blue) exhibit complementary trends, with dashed lines indicating reference levels.

 doi:10.20944/preprints202512.1749.v1

In p-polarization Figure 8a-b, the nanohole array shows a zero-crossing of the real permittivity near a filling fraction of ∼85%, while the nanopillar array exhibits a pole at a similar filling ratio. These features correspond to the effective medium's transition between dielectric and metallic responses rather than direct evidence of physical resonances. Under s-polarization Figure 8c-d, both arrays exhibit monotonic trends in real and imaginary permittivity, with reduced sensitivity to geometry, consistent with the symmetric distribution of the electric field relative to the surface.

However, these observations should not be interpreted as direct demonstrations of ENZ or EOT phenomena. Instead, they highlight that polarization primarily influences the averaged dielectric response through anisotropic field distributions rather than through distinct resonant coupling mechanisms. The complementary trends between NH and NP structures under *s*-polarization suggest that polarization can modulate the effective refractive index in a controlled but limited manner. For sensing applications, the relatively uniform response under s-polarization implies higher stability and repeatability, whereas p-polarization remains more sensitive to geometry and material dispersion, o ering tunability at the cost of greater variability. Thus, polarization control rather than structural redesign can serve as a practical means to optimize the optical response of metasurface-based SPR sensors within the valid range of the EMT approximation.

These results are obtained using the Maxwell–Garnett effective medium approximation and are intended to illustrate qualitative polarization-dependent trends rather than exact resonance conditions.

4. Discussion

The EMT-TMM framework established here has been benchmarked against classical SPR data and provides a consistent analytical basis for describing filling-fraction–dependent plasmonic behavior in nanostructured Au metasurfaces. The EMT–TMM formalism established herein constitutes a fully analytical-numerical framework that accurately reproduces canonical surface plasmon resonance (SPR) conditions in the Kretschmann geometry. The consistency of the predicted resonance angles and reflectance profiles with established analytical and experimental data reported in Refs. [15,24] validates the physical soundness of the present approach. The chosen Au and Ti thicknesses therefore represent realistic parameters for Kretschmann-type architectures, ensuring that the analytical conclusions remain directly transferable to experimental fabrication conditions. As such, the study achieves full theoretical closure without requiring further empirical input.

Future extensions involving full-wave modeling or device fabrication will serve to apply, rather than verify, the foundational relations demonstrated here. Nevertheless, the homogenization assumption limits its quantitative accuracy for structures with features approaching the optical wavelength. To validate the present analytical trends, future work will integrate full-wave electromagnetic simulations including finite-difference time-domain (FDTD) and finite-element method (FEM) models to resolve near field distributions and compare angular reflectance minima with those predicted here. In parallel, angle-resolved reflectance and transmission spectroscopy will be performed on fabricated Ti/Au thin films and nanopillar/nanohole arrays to experimentally verify the predicted shifts in resonance angle and effective permittivity trends. This combined analytical, numerical, and experimental program will establish quantitative bounds for the EMT–TMM approach and enable predictive modeling of metasurface-based SPR sensors.

5. Conclusions

In this work, we systematically investigated the plasmonic behavior of gold-based metasurfaces composed of nanoholes and nanopillars, employing the Effective Medium Theory (EMT), the Transfer Matrix Method (TMM), and polarization-resolved analysis. Our results demonstrate that both the real and imaginary parts of the effective permittivity are strongly governed by the geometric parameters and the volume filling fraction of the nanostructures.

For p-polarization, nanoholes and nanopillars exhibit distinct plasmonic responses due to their respective cavity-like and protruding geometries. Nanohole arrays enhance electric field localization

 doi:10.20944/preprints202512.1749.v1

and exhibit a transition toward negative effective permittivity with comparatively lower optical losses at small filling fractions, making them suitable for supporting Kretschmann-type surface plasmon resonance (SPR) coupling within the EMT–TMM approximation. In contrast, nanopillar arrays, while capable of supporting partially confined optical modes, present higher optical losses due to the increased imaginary part of the effective permittivity at larger filling fractions. Under s-polarized illumination, both nanohole and nanopillar arrays show monotonic and nearly overlapping effective permittivity trends, reflecting the symmetric distribution of the electric field relative to the surface. In this regime, the electromagnetic response is dictated primarily by the volumetric gold content, rendering the effective optical behavior largely independent of detailed structural topology. This polarization-induced symmetry yields a stable and repeatable optical response, suggesting that s-polarization may be exploited for high-stability, geometry-insensitive SPR sensing. Overall, the results indicate that polarization control can be used as a practical and non-structural tuning parameter for optimizing plasmonic coupling in metasurface-based SPR sensors. Rather than demonstrating new resonance mechanisms, this work establishes a qualitative and validated analytical framework for interpreting how polarization and filling fraction jointly govern effective permittivity and macroscopic optical response in nanostructured gold metasurfaces.

Author Contributions: Conceptualization, R.C.M. and E.M.G.; methodology, R.C.M. and E.M.G.; software, K.K.S., P.M.V.G. and G.E.S.G.; validation, E.M.G., E.M.G. and R.C.M.; formal analysis, E.M.G. and R.C.M.; investigation, C.A.F.H. and R.C.M.; resources, E.M.G.; data curation, C.A.F.H. and M.T.R.C.; writing original draft preparation, E.M.G.; writing—review and editing, E.M.G. and R.C.M.; visualization, C.A.F.H.; supervision, R.C.M.; project administration, E.M.G. and R.C.M.; funding acquisition, E.M.G.

Funding: R.C.M.thanks to Consejo Nacional de Ciencia y Tecnologa by its funding through Basic Scientific Research Grant 475 A1-S-13587. E.M.G. also acknowledge the computer resources, technical expertise, and support provided by the Laboratorio Nacional de Cómputo de Alto Desempeño (LANCAD) through Project No. LANCAD-UAM-35-2024.

Acknowledgments: R.C.M. thanks to Consejo Nacional de Ciencia y Tecnología for its funding through Basic Scientific Research Grant 475 A1-S-13587. E.M.G. also acknowledges the computer resources, technical expertise, and support provided by the Laboratorio Nacional de Cómputo de Alto Desempeño (LANCAD) through Project No. LANCAD-UAM-35-2024."

Conflicts of Interest: Declare conflicts of interest or state "The authors declare no conflicts of interest.

References

1. Senanayake, P.; Hung, C.H.; Shapiro, J.; Lin, A.; Liang, B.; Williams, B.S.; Huffaker, D.L. Surface Plasmon-Enhanced Nanopillar Photodetectors. *Nano Lett.* **2011**. https://doi.org/10.1021/nl202732r.
2. Nakamoto, K.; Kurita, R.; Niwa, O. Arrays of Metallic Nanopillars in Holes for Plasmonic Devices. In Proceedings of the 15th International Conference on Miniaturized Systems for Chemistry and Life Sciences (MicroTAS), 2011, pp. 1786–1788.
3. Parsons, J.; Hendry, E.; Burrows, C.P.; Auguié, B.; Sambles, J.R.; Barnes, W.L. Localized Surface-Plasmon Resonances in Periodic Nondiffracting Metallic Nanoparticle and Nanohole Arrays. *Phys. Rev. B* **2009**, *79*, 073412. https://doi.org/10.1103/PhysRevB.79.073412.
4. Eftekhari, F.; Escobedo, C.; Ferreira, J.; Duan, X.; Girotto, E.M.; Brolo, A.G.; Gordon, R.; Sinton, D. Nanoholes as Nanochannels: Flow-Through Plasmonic Sensing. *Anal. Chem.* **2011**, *83*, 828–833. https://doi.org/10.1021/ac1025363.
5. Lesuffleur, A.; Im, H.; Lindquist, N.C.; Lim, K.S.; Oh, S.H. Laser-Illuminated Nanohole Arrays for Multiplex Plasmonic Microarray Sensing. *Opt. Express* **2008**, *16*, 219–224. https://doi.org/10.1364/OE.16.000219.
6. Lospinoso, D.; Colombelli, A.; Lomascolo, M.; Rella, R.; Manera, M.G. Self-Assembled Metal Nanohole Arrays with Tunable Plasmonic Properties for SERS Single-Molecule Detection. *Nanomaterials* **2022**, *12*, 380. https://doi.org/10.3390/nano12030380.
7. Kotlarek, D.; Fossati, S.; Venugopalan, P.; Quilis, N.G.; Slabý, J.; Homola, J.; Lequeux, M.; Amiard, F.; Lamy de la Chapelle, M.; Jonas, U.; et al. Actuated Plasmonic Nanohole Arrays for Sensing and Optical Spectroscopy Applications. *Nanoscale* **2020**, *12*, 9756–9768. https://doi.org/10.1039/d0nr00761g.

 doi:10.20944/preprints202512.1749.v1

8. Wang, W.; Cui, Y.; Fung, K.H.; Zhang, Y.; Ji, T.; Hao, Y. Comparison of Nanohole-Type and Nanopillar-Type Patterned Metallic Electrodes Incorporated in Organic Solar Cells. *Nanoscale Res. Lett.* **2017**, *12*, 538. https://doi.org/10.1186/s11671-017-2310-7.
9. Najiminaini, M.; Ertorer, E.; Kaminska, B.; Mittler, S.; Carson, J.J. Surface Plasmon Resonance Sensing Properties of a 3D Nanostructure Consisting of Aligned Nanohole and Nanocone Arrays. *Analyst* **2014**, *139*, 1876–1882. https://doi.org/10.1039/C3AN02332J.
10. Escobedo, C.; Vincent, S.; Choudhury, A.I.K.; Campbell, J.; Brolo, A.G.; Sinton, D.; Gordon, R. Integrated Nanohole Array Surface Plasmon Resonance Sensing Device Using a Dual-Wavelength Source. *J. Micromech. Microeng.* **2011**, *21*, 115001. https://doi.org/10.1088/0960-1317/21/11/115001.
11. Xiang, G.; Zhang, N.; Zhou, X. Localized Surface Plasmon Resonance Biosensing with Large Area of Gold Nanoholes Fabricated by Nanosphere Lithography. *Nanoscale Res. Lett.* **2010**, *5*, 818–822. https://doi.org/10.1007/s11671-010-9566-5.
12. Correia-Ledo, D.; Gibson, K.F.; Dhawan, A.; Couture, M.; Vo-Dinh, T.; Graham, D.; Masson, J.F. Assessing the Location of Surface Plasmons Over Nanotriangle and Nanohole Arrays of Different Size and Periodicity. *J. Phys. Chem. C* **2012**, *116*, 6884–6892. https://doi.org/10.1021/jp3009018.
13. Bicket, I.C.; Bellido, E.P.; McRae, D.; Kapetanovic, V.; Lagugné-Labarthet, F.; Botton, G.A. Surface Plasmon Resonance Mode Behaviour in Sierpinski Fractal Triangles and New Plasmonic Materials. *Microsc. Microanal.* **2019**, *25*, 636–637. https://doi.org/10.1017/S143192761900391X.
14. Jones, D.; Liu, N.; Corbett, B.; Lovera, P.; Quinn, A.J.; O'Riordan, A. Surface Plasmon Assisted Extraordinary Transmission in Metallic Nanohole Arrays and Its Suitability as a Bio-Sensor. *J. Phys.: Conf. Ser.* **2011**, *307*, 012005. https://doi.org/10.1088/1742-6596/307/1/012005.
15. Maier, S.A. *Plasmonics: Fundamentals and Applications*; Springer: New York, 2007.
16. Sarid, D.; Challener, W. *Modern Introduction to Surface Plasmons: Theory, Mathematica Modeling, and Applications*; Cambridge University Press: Cambridge, 2010.
17. Gupta, B.D.; Srivastava, S.K.; Verma, R.K. *Fiber Optic Sensors Based on Plasmonics*; World Scientific Publishing: Singapore, 2015.
18. Oulton, R. Surface plasmon laser: sources of nanoscopic light. *Materials Today.* **2012**, *15*, 26–34. https://doi.org/10.1016/S1369-7021(12)70018-4.
19. Barnes, W.L.; Dereux, A.; W, E.T. Surface plasmon subwavelength optics. *Nature* **2003**, *424*, 824–830. https://doi.org/10.1038/nature01937.
20. Chunguang, D.; Qingli, J.; Zhengfeng, H. Coupler-free transition from light to surface plasmon polariton. *Physics Review A* **2015**, *91*, 1–9. https://doi.org/10.1103/PhysRevA.91.013817.
21. Ebbesen, T.W.; Genet, C.; Bozhevolnyi, S. Surface-plasmon circuitry. *Physics Today* **2008**, *61*, 44–50. https://doi.org/10.1063/1.2930735.
22. Bliokh, K.Y.; Bekshaev1, A.Y.; Nori, F. Optical momentum and angular momentum in complex media: from the Abraham–Minkowski Debate to Unusual Properties of Surface Plasmon. *New Journal of Physics* **2017**, *19*, 1–23. https://doi.org/10.1088/1367-2630/aa8913.
23. H., R., Ed. *Surface Plasmons on Smooth and Rough Surfaces and on Gratings*; Vol. 111, *Springer Tracts in Modern Physics*, Springer Berlin, Heidelberg: Singapore, 1988.
24. Gwon, H.R.; Lee, S.H. Spectral and Angular Response of Surface Plasmon Resonance Based on the Kretschmann Prism Configuration. *Mat. Trans.* **2010**, *51*, 1150–1155. https://doi.org/10.2320/matertrans.M2010003.
25. Garibello, B.; Martin, Y. Deduction of Electric Field Module in a Multilayer of Isotropic Materials to Detect Surface Plasmons with a Graphical User Interface. *Jour. of Micr., Opt. and Electromagn. App.* **2021**, *20*, 1150–1155. https://doi.org/10.1590/2179-10742021v20i1927.
26. Kumar, M.; Prasad, S. Mid-infrared Biosensor Based on Bloch Surface Mode Excitation in Truncated One-Dimensional Ternary Photonics Crystal Under Kretschmann Configuration. *Plasm.* **2021**, *16*, 923–932. https://doi.org/10.1007/s11468-020-01331-3.
27. Babaei, F.; Seyyedi, S.A. Excitation of Surface Plasmon Both Interfaces of a Silver Thin Film in Two- Layer Kretschmann Geometry. *Plasm.* **2021**, *16*, 2139–2146. https://doi.org/10.1007/s11468-021-01476-9.
28. Laurio, C.M.; Katsuki, H.; Yanagi, H. Numerical Simulations on Strong Coupling of Bloch Surface Waves and Exciton in Dielectric-Semiconductor Multilayerd. *Journ. of Phys.: Cond. Matter.* **2020**, *32*, 415003–415008. https://doi.org/10.1088/1361-648X/ab9d48.

 doi:10.20944/preprints202512.1749.v1

29. Fen, Y.W.; Yunus, M.M. Optical Characterization of Multilayers Thin Films Using Surface Plasmon Resonance Method From Electromagnetic Theory to Sensor Application. *AIP Conf. Procc.* **2012**, *1482*, 132–135. https://doi.org/10.1063/1.4757452.
30. Wang, W.; Qi, L. L.
31. Collin, S. Nanostructure Arrays in Free-Space: optical Properties and Applications, journal = Rep. Prog. Phys., year = 2014, volume = 77, pages = 1–33, number = 126402, doi = 10.1088/0034-4885/77/12/126402.
32. Mulyanti, B.; Wulandari, C.; Mohamad, N.R.; Rifaldi, E.; Hasanah, L.; Menon, P.S. Bimetallic Ag/Au Thin Films in Kretschmann-Based Surface Plasmon Resonance Sensor for Glucose Detection. *Optoelectron. Adv. Mater. Rapid Commun.* **2020**, *14*, 487–493.
33. Kim, W.M.; Kim, S.H.; Lee, K.S.; Lee, T.S.; Kim, I.H. Titanium Nitride Thin Film as an Adhesion Layer for Surface Plasmon Resonance Sensor Chips. *Appl. Surf. Sci.* **2012**, *261*, 749–752. https://doi.org/10.1016/j.apsusc.2012.08.093.
34. Khairulazdan, N.B.; Mohamed, R.; Berhanuddin, D.D.; Menon, P.S. Characterisation of Nano-Thin Film GO/TiO_2 Layers for Kretschmann-Based Surface Plasmon Resonance Visible Sensing Using FDTD Method. *Opt. Appl.* **2021**, *51*, 579–587. https://doi.org/10.37190/oa210409.
35. Maier, S.A., Ed. *World Scientific Handbook of Metamaterials and Plasmonics*; Vol. 1, *World Scientific Series in Nanoscience and Nanotechnology*, World Scientific Publishing: Singapore, 2017.
36. Sareni, B.; Krähenbühl, L.; Beroual, A.; Brosseau, C. Effective dielectric constant of periodic composite materials. *Appl. Phys.* **1996**, *80*, 1688–1696. https://doi.org/10.1063/1.362969.